Published in final edited form as:
J Am Chem Soc. 2013 January 30; 135(4): 1617–1624. doi:10.1021/ja312353e.

Transforming thymidine into a magnetic resonance imaging probe for monitoring gene expression

Amnon Bar-Shir[1,2], **Guanshu Liu**[1,3], **Yajie Liang**[1,2], **Nirbhay N. Yadav**[1,3], **Michael T. McMahon**[1,3], **Piotr Walczak**[1,2], **Sridhar Nimmagadda**[4], **Martin G. Pomper**[4], **Keri A. Tallman**[5], **Marc M. Greenberg**[5], **Peter C.M. van Zijl**[1,3], **Jeff W.M. Bulte**[1,2,6,7], and **Assaf A. Gilad**[1,2,3,*]

[1]Division of MR Research, Russell H. Morgan Department of Radiology, The Johns Hopkins University School of Medicine, Baltimore, MD, United States

[2]Cellular Imaging Section, Institute for Cell Engineering, The Johns Hopkins University School of Medicine, Baltimore, MD, United States

[3]F.M. Kirby Research Center for Functional Brain Imaging, Kennedy Krieger Institute, Baltimore, MD, United States

[4]Russell H. Morgan Department of Radiology, The Johns Hopkins University School of Medicine, Baltimore, MD, United States

[5]Department of Chemistry, The Johns Hopkins University, Baltimore, MD, United States

[6]Department of Biomedical Engineering, The Johns Hopkins University, Baltimore, MD, United States

[7]Department of Chemical & Biomolecular Engineering, The Johns Hopkins University, MD, United States

Abstract

Synthetic chemistry has revolutionized the understanding of many biological systems. Small compounds that act as agonists and antagonists of proteins, and occasionally as imaging probes, have contributed tremendously to the elucidation of many biological pathways. Nevertheless, the function of thousands of proteins is still elusive, and designing new imaging probes remains a challenge. Through screening and characterization we identified thymidine analog as probe for imaging the expression of the Herpes Simplex Virus type-1 thymidine kinase (HSV1-TK). To detect the probe, we used chemical exchange saturation transfer magnetic resonance imaging (CEST-MRI), in which a dynamic exchange process between an exchangeable proton and the surrounding water protons is used to amplify the desired contrast. Initially, five pyrimidine-based molecules were recognized as putative imaging agents, since their exchangeable imino protons resonate at 5–6ppm from the water proton frequency and their detection is therefore less affected by endogenous CEST contrast or confounded by direct water saturation. Increasing the pK_a value of the imino proton by reduction of its 5,6-double bond results in a significant reduction of the exchange rate (k_{ex}) between this proton and the water protons. This reduced k_{ex} of the dihydropyrimidine nucleosides fulfills the “slow to intermediate regime” condition for generating high CEST-MRI contrast. Consequently, we identified 5-methyl-5,6-dihydrothymidine as the

*Corresponding author: Assaf A. Gilad, Ph.D., The Johns Hopkins University School of Medicine, 1550 Orleans St., Cancer Research Building II, Room 4M63, Baltimore, MD 21231. Phone: 410-502-8188, Fax: 410-614-1948, assaf.gilad@jhu.edu.

Supporting Information Available

Simulations of CEST data, In vitro imaging using a clinical 3 Tesla MRI scanner, call viability and apoptosis assays, phosphorylation effect on CEST data and raw SPECT images are included in the Supporting Information. This material is available free of charge via internet at http://pubs.acs/org.

optimal probe and demonstrated its feasibility for *in vivo* imaging of the HSV1-TK. In light of these findings, this new approach can be generalized for designing specific probes for the *in vivo* imaging of a variety of proteins and enzymes.

1. Introduction

The herpes simplex virus type-1 thymidine kinase (HSV1-TK) is a viral enzyme that catalyzes the synthesis of thymidine monophosphate. Compared to mammalian thymidine kinases, HSV1-TK has a lower substrate specificity, and thus phosphorylates an array of therapeutics and imaging agents. These applications rely on the entrapment and accumulation of the phosphorylated nucleoside only in cells expressing the HSV1-TK[1]. Radiolabeled nucleosides are widely used as imaging probes for HSV1-TK expression with positron emission tomography (PET) and single photon emission computed tomography (SPECT) in [1–4].

The imaging probes for magnetic resonance imaging (MRI) are termed “contrast agents” since they enhance the water-proton-based contrast between the imaging target and surrounding tissue. Recently, a new type of contrast mechanism has been developed that exploits chemical exchange saturation transfer (CEST)[5–7], to indirectly detect low-concentration solutes through the water signal used for MRI. CEST-MRI contrast is generated by applying a selective radio-frequency pulse (saturation pulse) that annihilates the magnetization of specific protons on the solute. Due to dynamic chemical exchange of the “saturated” protons with the water protons and continuous replacement of saturated protons by unsaturated protons followed by renewed saturation, the net magnetization of the water proton is progressively reduced, thus enhancing the MRI contrast. This new contrast mechanism has been used in a range of applications using either diamagnetic (DIACEST) or paramagnetic (PARACEST) agents[5,6,8].

CEST contrast is highly dependent on the exchange rate (k_{ex}) of the saturated protons with the water protons. In order to achieve the highest contrast and specificity, k_{ex} should preferably be fast, but in the “slow exchange regime” on the NMR time scale, as defined by $k_{ex} \ll \Delta\omega$, where $\Delta\omega$ is the chemical shift difference between the resonance frequency of the exchangeable protons and the water protons[5,6,9]. One main drawback of DIACEST agents therefore is the small $\Delta\omega$ between their exchangeable protons (i.e., $\Delta\omega < 4$ ppm for amide, amine, guanidine, and hydroxyl protons) and the water protons. This may lead to deleterious effects from direct saturation of the water protons and increased background signal from endogenous exchangeable protons[10–13]. The imino proton of pyrimidine-based nucleosides has a $\Delta\omega$=5–6ppm[14], making pyrimidine analogues potentially suitable for CEST imaging. However, k_{ex} of the imino protons with water is fast (>3000 s^{-1}) and thus needs to be reduced in order to make these nucleosides ideal CEST-based contrast agents. Changing the acid dissociation constant (pK_a) value of the imino proton of dT by rational chemical modification can be used to modulate its k_{ex}. We therefore modified dT chemically to improve its CEST MRI properties by increasing the imino proton pK_a value and reducing its k_{ex} with water to comply with the slow exchange condition on the NMR time scale. The synthetic dT analog, 5-methyl-5,6-dihydrothymidine, showed an excellent CEST contrast, as well as high specificity to HSV1-TK, and allowed successful *in vivo* monitoring of HSV1-TK expression in tumors with MRI.

2. Experimental Section

See Supporting Information text for detailed descriptions of following methods: (i) Simulations of CEST data, (ii) CEST-MRI at 3.0 Tesla clinical MRI scanner, (iii) cell

viability assay, (iv) cell uptake assay, (v) terminal transferase nick-end-labeling (TUNEL) assay.

2.1 CEST imaging probes

5-methyl-5,6-dihydrothymidine (**2**) and thymidine glycol (**3**) were prepared as previously described[15,16]. Thymidine (dT) and 5-Chloro-2′-deoxyuridine (**4**) were purchased from Sigma-Aldrich Co. and (5S)-5,6-dihydrothymidine (**1**) was purchased from Berry & Associates, Inc.

2.2 Cloning

The HSV1-*tk* gene was cloned into pEXP-5-CT (Invitrogen) for expression in *E. coli* (pEXP-5-CT-HSV1-*tk*). For mammalian expression, the gene was cloned into pcDNA3.1 (Invitrogen; pcDNA3.1-HSV1-*tk*) and pLenti-6- V5/DEST vector (Invitrogen; pLenti-6-HSV1-*tk*), both under a cytomegalovirus (CMV) promoter and a fused V5-tag.

2.3 HSV1-TK Expression and purification

BL21 (DE3) (Invitrogen) cells were transformed with pEXP-5-CT-HSV1-*tk*. After induction in Magic Media™ (Invitrogen) at 30°C for 18 hours, the total protein was extracted and the recombinant HSV1-TK protein fused to the six-histidine tag, and purified using cobalt-based immobilized metal affinity chromatography (HisPur Cobalt Resin, Thermo Scientific). The expression and purity was determined by SDS-polyacrylamide gel electrophoresis (SDS-PAGE) and was validated by Western blot using an anti-His antibody (Invitrogen).

2.4 Expression in mammalian cells

Viruses were propagated in Human Embryonic Kidney 293 cells (HEK-293FT). Forty-eight hours after transduction, cells were lysed using Mammalian Protein Extraction Reagent (Thermo Scientific Inc.), and anti-V5 antibody (Invitrogen) was used for immunofluorescence and western blot analyses.

2.5 pKa Values

The pKa values of the imino protons for the examined molecules, were calculated using ChemAxon MarvinSketch v.5.3.3 software (www.chemaxon.com/marvin).

2.6 Kinase assay

In a solid white 96-well plate, 5 μM substrate (dT, compounds **1**, **2** or **3**, N=4 for each substrate) and 20 μM ATP were dissolved in 48 μl of kinase reaction buffer (40 mM Tris; pH=7.5, 20 mM $MgCl_2$, and 0.1 mg/ml BSA) followed by the addition of 2 μl of purified HSV1-TK to initiate the kinase reaction. Eight wells without substrate were included as control reference. The plate was incubated at room temperature for 2h, after which 50μl Kinase-Glo luciferase reagent (Kinase-Glo® Max Luminescent Kinase Assay, Promega Inc.) were added. After 30 min, the resulting luminescence values were recorded and used to quantity the residual ATP in the reaction. The relative phosphorylation (%) was then defined as the luminescence signal obtained after the enzymatic reaction (Substrate + HSV1-TK + ATP) relative to the signal obtained from wells without substrate (HSV1-TK+ ATP). For a phosphorylation assay performed on HEK293FT lysates, 2 μl of cell extract (either $293^{HSV1\text{-}tk}$ or 293^{wt} cells) were used instead of purified HSV1-TK, and the assay was performed using **1** or **2** as substrates according to the procedure described above.

2.7 *In vitro* CEST-MRI

All compounds were dissolved at a concentration of 20 mM in PBS (pH=7.4) and placed in micro-capillaries, as described previously [17]. CEST-MRI experiments were performed on a vertical 11.7 Tesla scanner (Bruker Avance system) at 37°C. A modified RARE sequence (TR/TE=10,000/9.4 ms, RARE factor=16, 1 mm slice thickness, FOV=11×11 mm, matrix size=64×32, resolution=0.17×0.34 mm, and NA=2) including a magnetization transfer (MT) module (B_1/t_{sat} = 170 Hz/4000 ms) was used to acquire CEST-weighted images from −8 to +8 ppm with increments of 0.2 ppm around the water resonance, which was assigned to be at 0 ppm. Pixel-based B_0 correction was used as described before[18] using the same parameters as above except for TR=1500 ms, B_1/t_{sat} = 21 Hz/500ms, with a sweep range from −2 to +2 ppm (0.1 ppm steps). Data processing was performed using custom-written scripts in MATLAB® (Mathworks). Mean CEST spectra were plotted from an ROI for each sample, after B_0 correction. $MTR_{asym}=100\times(S^{-\Delta\omega} - S^{\Delta\omega})/S_0$ was computed at different offsets Uω.

2.8 Quantification of exchange rates

Exchange rates were quantified with the saturation power dependent CEST approach (QUESP) and Bloch equation fitting[19]. For each sample, the MTR_{asym} was measured at the imino resonance frequency for CEST saturation fields of 43, 85, 128, 170, 213, 255, 340, and 426 Hz while the saturation pulse duration was kept constant at 4000 ms. The Bloch equations were then fit numerically to these MTR_{asym} values using MATLAB® (Mathworks) and the exchange rates (k_{ex}, sec^{-1}) were determined from the fits. Errors (95% confidence limits) were estimated using the *F* statistic.

2.9 Cell transfection and transplantation

pcDNA3.1-HSV1-*tk* was used to transfect 9L rat glioma cells. Single clones of ($9L^{HSV1\text{-}tk}$), were selected with 0.5mg/ml of G418 antibiotics. $9L^{HSV1\text{-}tk}$ and non-transfected wild type 9L cells ($9L^{wt}$) were inoculated (2×10^5 cells/2μl saline) bilaterally into the striatum of adult NOD-SCID male mice to generate intracranial 9L tumors in both hemispheres.

2.10 *In vivo* CEST-MRI

Data were acquired using a horizontal 11.7 Tesla MRI scanner (Bruker, Biospec) equipped with a circular polarized MRI transceiver coil (ID = 23mm). Seven days after cell transplantation, mice were anesthetized with 1.5% isoflurane and a series of four CEST data sets were obtained at one hour, two hours, and three hours following i.v. injection of **2** in saline (150 mg/kg body). CEST-weighted images were acquired with a modified RARE pulse sequence (TR/TE = 6000/35ms), using a 213Hz/4000ms saturation pulse alternating between ±5ppm frequency offsets from the water frequency. For each time point, the MTR_{asym} map was calculated from four pairs of S^{-5ppm}/S^{+5ppm} using MATLAB® (Mathworks). A single 1 mm slice with FOV of $1.6\times1.6cm^2$ and a 128 ×48 matrix was used. To remove magnetization transfer effects ΔMTR_{asym} was defined as [MTR_{asym} (tumor)]−[MTR_{asym} (normal brain tissue)] as previously suggested[20].

2.11 Immunofluorescent histology

Mice were transcardially perfused with 10 mM PBS, followed by 4% paraformaldehyde (PFA) fixation. Brains were removed and fixed in 4% PFA overnight, cryopreserved in 30% sucrose, and followed by cryo-sectioning at 30 μm slices. Brain slices were blocked for one hour at room temperature with PBS containing 5% bovine serum albumin (BSA), followed by overnight incubation in anti-V5 antibody solution. Nuclei were stained using 1 μg/mL DAPI (Invitrogen).

2.12 SPECT/CT

An X-SPECT small-animal SPECT/CT system (Gamma Medica-Ideas) was used for image acquisition as previously described[21]. Briefly, seven days after cell implantation, the mice were injected i.v. with 50.3 MBq (1.36 mCi) of $^{[125I]}$FIAU. SPECT data were acquired three hours after radiotracer injection and the obtained images were co-registered with the corresponding 512-slice CT images. Fused SPECT/CT transaxial sections of 1 mm thickness were generated using Amira 5.2.0 software (Visage Imaging Inc.) showing the SPECT signal obtained from the brain.

3. Results

3.1 Dihydrothymidines enhance the CEST contrast *in vitro*

Calculated and published pK_a values of the imino proton of dT and four of its analogs (Figure 1a) are summarized in Table 1. Upon hydrogenation of the 5–6 double bond of the pyrimidine ring, the pK_a value of the exchangeable imino proton increases from about 9.8 for dT[22] to 11.60 for 5,6-dihydrothymidine (**1**) due to the loss of the pyrimidine ring aromaticity. A methylation at position 5 of **1** produces 5-methyl-5,6-dihydrothymidine (**2**) and has a negligible effect on the pK_a of its imino proton (pK_a=11.57). The imino proton of thymidine glycol (**3**) has a pK_a of 11.0, just between dT and compounds **1** and **2**, due to its two additional hydroxyl electron-withdrawing groups at the pyrimidine ring. The substitution of the electron-donating methyl group of dT with an electron-withdrawing group, Cl, to generate 5-chloro-2′-deoxyuridine (**4**), reversed the inductive properties of the 5-substituent and considerably reduced the pK_a value of the imino proton to about 7.9[23].

Using an 11.7 Tesla MRI scanner, we compared the CEST contrast generated by solutions of these four deoxynucleoside analogs in phosphate-buffered saline (PBS, pH=7.4, 37°C) with that of dT. The solid lines in Figure 1c–f represent the CEST spectra, in which the water proton signal (S), normalized by the unsaturated signal (S_0), is plotted as a function of saturation frequency with respect to the water proton resonance frequency. This convention of assigning 0 ppm to the water protons is used in CEST MRI and should not be confused with proton spectroscopy, in which the water resonance is assigned with respect to tetramethylsilane (TMS) or trimethylsilyl propanoic acid (TSP) and resonates around 4.7–4.8ppm. The dashed lines represent plots of the asymmetry in the magnetization transfer ratio (MTR_{asym}), a measure of CEST contrast defined by: $MTR_{asym} = 100\% \times (S^{-U\omega} - S^{+U\omega})/S_0$, where $S^{-U\omega}$ and $S^{+U\omega}$ are the MRI signal intensities after saturation at $-U\omega$ and $+U\omega$ with respect to the water proton frequency. Taking the signal difference at $-U\omega$ and $+U\omega$ can remove confounding effects due to direct saturation of the water protons. The imino protons of compounds **1–3** showed a local maximum contrast at 5 ppm downfield of the water proton frequency, but only the dihydrothymidines (**1** and **2)** showed a well-defined sharp peak at that frequency (Figure 1c–f).

Higher exchange rates increase the magnitude of the CEST contrast, which consequently improves the probe's sensitivity. However, if the exchange rate is too fast, the exchanging protons already exchange before being saturated by the CEST labeling pulse. Additionally, for fast exchange rates, the imino and water proton peaks can merge and thus the imino signal cannot be distinguished from the water signal. The maximal contrast (slow exchange regime) should be achievable by using an optimal saturation field (B_1) that can be predicted by the expression, $B_1(\text{optimal}) = k_{ex}/2\pi$[24]. To assess this, we quantified k_{ex} in the newly designed probes from the saturation power dependencies of the MTR_{asym} values[19] at 5 ppm for **1–3,** and at 6 ppm for dT (Figure 1g–j, Table 1). The imino protons of the two dihydrothymidines, which have the highest pK_a values (**1** and **2**; Table 1), best fulfill the "slow exchange regime" rule with k_{ex} values of $0.8\pm0.2 \times 10^3 s^{-1}$ and $1.7\pm0.3\times10^3 s^{-1}$,

respectively, for a chemical shift of $\Delta\omega$ = 5ppm (=1.6×10^4 rad/s at 11.7 Tesla). The calculated optimal saturation fields (B_1) were 127 Hz for **1** and 270 Hz for **2**. In fact, the MTR_{asym} values of both compounds **1** and **2**, reach a plateau at higher B_1 (Figure 1g,h), when saturation fields increase above the optimal value. The imino proton of compound **3** is approaching the intermediate exchange rate range (k_{ex} = $3.7\pm0.2\times10^3 s^{-1}$), and therefore, shows a broadening of the MTR_{asym} curve compared to **1** or **2** (Figure 1c–e). However, as predicted[24], it produces a higher MTR_{asym} if a higher B_1 is used (Figure 1i). No CEST contrast was observed from the imino proton of compound **4** (Table 1, Figure 1b,f), which has the lowest pK_a value (7.97) and falls in the fast exchange regime ($k_{ex} \gg \Delta\omega$) on the NMR time scale.

The results in Figure 1 obtained using an MRI scanner operating at field strength of 11.7 Tesla. To evaluate the feasibility of imaging dihydrothymidines at clinical MRI lower field strengths typically used in clinical MRI, we simulated (for dT and compounds **1–3**) and performed (dT and **1**) CEST experiments at 3 Tesla. The results were compared to simulations and experimental data at 11.7 Tesla. Compounds **1** and **2** fulfill the $k_{ex}\delta\Delta\omega$ condition at both 11.7 and 3.0 Tesla and showed a distinct peak at the 5ppm offset from the water frequency for the two magnetic field strengths (Figure S1 a,b and c,d). In contrast, for **3** and dT, which have a faster exchanging imino proton ($5.1\pm0.7\times10^3$ s^{-1} and $3.7\pm0.2\times10^3$ s^{-1}, respectively, Table 1), no peak could be distinguished at the simulated CEST data for the lower magnetic field (Figure S1 d and f), where the $k_{ex}\delta\Delta\omega$ condition is not fulfilled for B_0=3.0 Tesla. As mentioned, **1** fulfills the $k_{ex}\delta\Delta\omega$ condition at 3.0 Tesla and thus, produces a visible peak at the 5ppm offset from the water frequency at the CEST experimental data (Figure S2b), as has been predicted by the simulations (Figure 1Sb). In contrast, for dT, which has a faster exchanging imino proton no peak could be distinguished and the MTR_{asym} value at 5ppm obtained for **1** was 40% higher compared to dT (Figure S2a).

3.2 The dihydrothymidines are phosphorylated by HSV1-TK

A major obstacle in designing new imaging probes is to maintain functionality after chemical modification. Therefore, we examined the phosphorylation level of each compound by recombinant purified HSV1-TK. The HSV1-*tk* gene was subcloned into the pEXP5-CT expression vector in a reading frame with a C-terminal six-histidine tag and subsequently transformed into BL21 (DE3) chemically competent *E. coli*. The recombinant HSV1-TK enzyme was expressed and purified using cobalt-based immobilized metal affinity chromatography (Figure 2a). Notably, the observed phosphorylation of dT and analogs **1** and **2** by purified HSV1-TK was similar (>57%, Figure 2b) after two hours incubation in the presence of ATP as the donor phosphate group. However, a lower degree of phosphorylation was observed for **3** (17%; Figure 2b), which may be explained by the hydrophobic nature of the HSV1-TK nucleoside binding site[29]. Overall, these results demonstrate that **1** and **2**, which yield CEST contrast that is superior to dT, can serve as CEST-based contrast agents for HSV1-TK, despite their chemical modification.

Next, we examined whether the contrast is affected by phosphorylation. We measured the CEST contrast, with or without purified HSV1-TK, incubated in the presence of ATP for two hours incubation at 37°C (pH=7.4), followed by 20 min heat-inactivation of the enzyme at 65°C to end the kinase reaction. Since the phosphorylation site of the substrates is at the 5′-hydroxyl of the deoxyribose moiety, it is expected that the exchange rate of the imino proton, and consequently, the MTR_{asym} value at 5 ppm would not be affected by phosphorylation. Indeed, the CEST contrast was not affected by phosphorylation and the MTR_{asym} values at 5ppm were identical before and after the enzymatic reaction (Figure 2c,d, and Figure S3).

Additionally, we compared the phosphorylation specificity of HSV1-TK to endogenous mammalian thymidine kinases (m-TK) for compounds **1** and **2**. Toward that end, we constructed a lentivirus that encodes the HSV1-TK under the cytomegalovirus (CMV) promoter and transduced human embryonic kidney (HEK293FT) cells (Figure 3a–c). The protein extracts of transduced $293^{HSV1\text{-}tk}$ cells (containing both HSV1-TK and m-TK) and wild type (293^{wt}) control cells (containing m-TK only) were used to measure enzymatic activity in the presence of either **1** or **2**. Figure 3d demonstrates that cell extracts containing the HSV1-TK exhibited significantly higher phosphorylation of **1** and **2** than control cells. While compounds **1** and **2** had comparable phosphorylation rates, the increase in phosphorylation of **2** with respect to the control extract (293^{wt}) was greater by a factor of about ten than that of **1**, indicating that the additional methyl on position 5, which distinguishes **2** from **1**, improves its specificity for HSV1-TK over m-TK. These results are in agreement with the findings that different dT analogs showed variable levels of phosphorylation by m-TK[25]. Moreover, it is important to note that such phosphorylation of **2** did not show any toxic effect on the $293^{HSV1\text{-}tk}$ (Figure S4). This finding is in agreement with previous study showing that dihydrothymidines have no effect on DNA synthesis and do not increase the rate of mutations[26]. In contrast, the anti-viral prodrug ganciclovir (GCV) resulted in a cytotoxic effect to the $293^{HSV1\text{-}tk}$ upon phosphorylation (Figure S4) as predicted and been previously reported[27].

3.3 Imaging HSV1-TK activity *in vivo* with 5-methyl-5,6-dihydrothymidine

Next, we evaluated the feasibility of using 5-methyl-5,6-dihydrothymidine (**2**) as a CEST imaging probe for monitoring HSV1-TK *in vivo*. The rat glioma cell line (9L) was transfected with the expression vector, pcDNA™3.1, which encodes to HSV1-*tk* under the regulation of the CMV promoter. Following antibiotic selection, a single clone that showed stable expression levels of the enzyme was selected ($9L^{HSV1\text{-}tk}$). Wild type, non-transfected 9L cells were used as controls ($9L^{wt}$). The HSV1-TK expression in $9L^{HSV1\text{-}tk}$ cells was confirmed by immunofluorescence (Figure S5a,b). The HSV1-TK activity was evaluated by *in vitro* cell-uptake assay, in which a significance accumulation of the radioactive nucleoside [^{125}I]FIAU was observed in $9L^{HSV1\text{-}tk}$ cells after one and three hours incubation compared to $9L^{wt}$ cells (Figure S5c).

Inoculation of $9L^{HSV1\text{-}tk}$ to the ipsilateral striatum and $9L^{wt}$ into the contralateral striatum of adult male NOD-SCID mice (n=6) resulted in one tumor in each hemisphere of the brain. One week after tumor inoculation, analog **2** was injected intravenously (i.v.) and mice were scanned on a dedicated animal MRI scanner (11.7 Tesla, horizontal bore). Maps of MTR_{asym} were acquired at one, two and three hours post injection. Figure 4a shows representative longitudinal MTR_{asym} (5 ppm) maps. As depicts in Figure 4b three hours after injection of the probe the normalized mean MTR_{asym} values (ΔMTR_{asym}) from the $9L^{HSV1\text{-}tk}$ were significantly higher than those obtained from control tumors (4.8±1.5 for $9L^{HSV1\text{-}tk}$ and 2.5±1.8 for $9L^{wt}$; n=6; p=0.03). These findings indicate intracellular accumulation (approximately 0.7 mM, Figure S6-S8) in the $9L^{HSV1\text{-}tk}$ tumors as opposed to clearance from control tumors. Such accumulation of **2** did not induce apoptosis neither in $9L^{HSV1\text{-}tk}$ nor in $9L^{wt}$ as revealed by terminal deoxynucleotidyl transferase dUTP nick end labeling (TUNEL) staining (Figure S9). The HSV1-TK functionality was confirmed by the administration of radiolabeled [^{125}I]FIAU using SPECT/CT. In agreement with the CEST MRI results, accumulation of [^{125}I]FIAU was observed three hours after i.v. injection only at the $9L^{HSV1\text{-}tk}$ tumor (Figure 4c and S10). The high expression levels of the HSV1-TK in the $9L^{HSV1\text{-}tk}$ tumor was validated by immunofluorescence (Figure 4d).

Overall, these data demonstrate that 5-methyl-5,6-dihydrothymidine (**2**) can be used as an MRI probe to monitor HSV1-TK *in vivo*.

4. Discussion

We identified 5-methyl-5,6-dihydrothymidine (**2**) as a functional probe for imaging HSV1-TK with CEST. Its exchangeable imino proton, which resonates at $\Delta\omega = 5$ ppm, has a considerably lower k_{ex} than parent dT due to its higher pK_a value allowing CEST detection with optimal MRI specificity. In addition, while this compound is phosphorylated by the HSV1-TK, it is barely phosphorylated by endogenous kinases, and therefore, allows *in vivo* MRI of HSV1-*tk* gene expression with high functional specificity.

Due to the contribution of endogenous proteins and metabolites to *in vivo* CEST contrast following saturation in the $\Delta\omega$ range of 0–4 ppm from water[10–13], it is imperative to design an imaging probe with an exchangeable proton that resonates downfield to this crowded endogenous range. The imino protons of the synthetic deoxynucleosides **1** and **2**, not only resonate at $\Delta\omega = 5$ ppm, but also have a relatively slow k_{ex} compared to dT (Table 1) resulting in a well-defined peak centered at the CEST spectra. One advantage over previous generation of CEST reporter genes[28,29] is that the HSV1-TK CEST-based substrate provides a sharper signal at 5 ppm frequency offset. This makes **1** and **2** favorable DIACEST based reporters and contrast agents due to less interference from contrast originating in other probes that have exchangeable protons resonate at different frequencies e.g., amide protons at $\Delta\omega \approx 3.6$ ppm[13,28], amine protons at $\Delta\omega \approx 2–2.4$ ppm[10,29], guanidyl protons at $\Delta\omega \approx 1.5–1.8$ ppm[30], and hydroxyl proton at $\Delta\omega \approx 0.9$ ppm [11,12]. This may allow simultaneous imaging of multiple targets within the same sample[30] and therefore, may play an instrumental role in studying complex biological systems. The reduced k_{ex} of **1** and **2** allowed CEST detection not only at preclinical MRI scanners operating at high magnetic field (11.7 Tesla in this study) but also at 3.0 Tesla clinical scanner, where the condition $k_{ex} < \Delta\omega$ is maintained. However, for clinical MRI scanners, specific absorption rate (SAR) and hardware limitations currently prevent optimal CEST MRI measurements on low volume samples and small animals. We avoided these limitations in our 3 Tesla experiments by using a pulsed CEST approach[31] however this technique produces less CEST contrast compared to conventional CEST methods. It is important to note that chemical exchange can affect the transverse relaxation as was measured with NMR in solutions containing diamagnetic proteins and metabolites[32,33] This property was used for measuring the exchange rate of protein in solution[33]

MRI has been used in the past for studying HSV1-*tk* as a therapeutic gene. The activity of the HSV1-TK was measured as the outcome of treatment with GCV as was manifested by changes in T_2 and T_{1rho} [34,35]. In those cases, the changes were observed within 4 and two days respectively. Our results demonstrate that the HSV1-*tk* can be used as an MRI reporter gene for *in vivo* applications where the reporter activity is measured directly within hours. This is manifested by a statistically significant difference between the CEST contrast produced by $9L^{HSV1\text{-}tk}$ and $9L^{wt}$ tumors, three hours after injection of compound **2**. It is important to note that the kinetics of the imaging probe may vary between different biological systems or even among individual mice, for instance due to the heterogeneity of the tumor vasculature, which may alter the accumulation and clearance of the imaging probe. In addition, in order to improve the sensitivity of the suggested system for monitoring enzyme expression, mutated HSV1-TK, which is adjusted to have a higher V_{max}/K_m toward the imaging probe (**2**) and a lower V_{max}/K_m for dT, should be considered, in a manner similar to that applied for the PET imaging of HSV1-*tk* expression[36].

Since CEST contrast is visible only when a saturation pulse is applied, it may be used to evaluate multiple genes simultaneously using different MR reporter genes, including CEST reporter genes[28,29], paramagnetic MRI reporter genes that alter the transverse relaxation (T_2) of the tissue through accumulation of iron[37,38], or MRI-based reporter genes that are

designed for either ^{31}P- or ^{19}F- MR spectroscopy[39–41]. Furthermore, with the recent development of combined PET/MRI high-field scanners[42], combining CEST with nuclear imaging could open up new avenues for multi-modality molecular and cellular imaging.

5. Conclusion

In summary, we have identified an imaging probe that provides frequency-specific MRI contrast with high functional specificity to HSV1-TK. Thus, we have demonstrated, both *in vitro* and *in vivo,* the transformation of HSV1-*tk* into an MRI reporter gene. This imaging probe, which is stable for long periods, has the potential to allow serial monitoring of gene expression combined with high-resolution functional and anatomical MRI, as well as in conjunction with nuclear imaging. Overall, the principles outlined in this work may be further extended to a general paradigm for the design and synthesis of new imaging probes for *in vivo* imaging of a wide range of proteins *en route* to the elucidation of their biological function.

Supplementary Material

Refer to Web version on PubMed Central for supplementary material.

Acknowledgments

Supported by NIH grants EB008769, NS065284, EB005252, EB012590, EB015032, GM-054996 and MSCRFF-0103-00. The authors would like to thank Drs. Y. Kato, A.P. Pathak, G. Pelled, J. Xu, C.K. Jones L. Jiang, K. Glunde and R.D. Airan.

References

1. Tjuvajev JG, Stockhammer G, Desai R, Uehara H, Watanabe K, Gansbacher B, Blasberg RG. Cancer Res. 1995; 55:6126. [PubMed: 8521403]
2. Gambhir SS, Barrio JR, Phelps ME, Iyer M, Namavari M, Satyamurthy N, Wu L, Green LA, Bauer E, MacLaren DC, Nguyen K, Berk AJ, Cherry SR, Herschman HR. Proc Natl Acad Sci U S A. 1999; 96:2333. [PubMed: 10051642]
3. Jacobs A, Voges J, Reszka R, Lercher M, Gossmann A, Kracht L, Kaestle C, Wagner R, Wienhard K, Heiss WD. The Lancet. 2001; 358:727.
4. Yaghoubi SS, Jensen MC, Satyamurthy N, Budhiraja S, Paik D, Czernin J, Gambhir SS. Nat Clin Pract Oncol. 2009; 6:53. [PubMed: 19015650]
5. Sherry AD, Woods M. Annu Rev Biomed Eng. 2008; 10:391. [PubMed: 18647117]
6. van Zijl PC, Yadav NN. Magn Reson Med. 2011; 65:927. [PubMed: 21337419]
7. Ward KM, Aletras AH, Balaban RS. J Magn Reson. 2000; 143:79. [PubMed: 10698648]
8. Terreno E, Castelli DD, Aime S. Contrast Media Mol Imaging. 2010; 5:78. [PubMed: 20419761]
9. Ward KM, Aletras AH, Balaban RS. J Magn Reson. 2000; 143:79. [PubMed: 10698648]
10. Cai K, Haris M, Singh A, Kogan F, Greenberg JH, Hariharan H, Detre JA, Reddy R. Nat Med. 2012; 18:302. [PubMed: 22270722]
11. Ling W, Regatte RR, Navon G, Jerschow A. Proc Natl Acad Sci U S A. 2008; 105:2266. [PubMed: 18268341]
12. van Zijl PC, Jones CK, Ren J, Malloy CR, Sherry AD. Proc Natl Acad Sci U S A. 2007; 104:4359. [PubMed: 17360529]
13. Zhou J, Payen JF, Wilson DA, Traystman RJ, van Zijl PC. Nat Med. 2003; 9:1085. [PubMed: 12872167]
14. Snoussi K, Bulte JW, Gueron M, van Zijl PC. Magn Reson Med. 2003; 49:998. [PubMed: 12768576]
15. Barvian MR, Greenberg MM. J Org Chem. 1993; 58:6151.

16. Greenberg MM, Matray TJ. Biochemistry. 1997; 36:14071. [PubMed: 9369479]
17. Liu G, Gilad AA, Bulte JW, van Zijl PC, McMahon MT. Contrast Media Mol Imaging. 2010; 5:162. [PubMed: 20586030]
18. Kim M, Gillen J, Landman BA, Zhou J, van Zijl PC. Magn Reson Med. 2009; 61:1441. [PubMed: 19358232]
19. McMahon MT, Gilad AA, Zhou J, Sun PZ, Bulte JW, van Zijl PC. Magn Reson Med. 2006; 55:836. [PubMed: 16506187]
20. Zhou J, Lal B, Wilson DA, Laterra J, van Zijl PC. Magn Reson Med. 2003; 50:1120. [PubMed: 14648559]
21. Nimmagadda S, Pullambhatla M, Pomper MG. J Nucl Med. 2009; 50:1124. [PubMed: 19525448]
22. Dawson, RMC. Data for biochemical research. Clarendon Press; Oxford: 1959.
23. Theruvathu JA, Kim CH, Darwanto A, Neidigh JW, Sowers LC. Biochemistry. 2009; 48:11312. [PubMed: 19863157]
24. Woessner DE, Zhang S, Merritt ME, Sherry AD. Magn Reson Med. 2005; 53:790. [PubMed: 15799055]
25. Alauddin MM, Gelovani JG. Curr Med Chem. 2010; 17:1010. [PubMed: 20156163]
26. Evans J, Maccabee M, Hatahet Z, Courcelle J, Bockrath R, Ide H, Wallace S. Mutat Res. 1993; 299:147. [PubMed: 7683083]
27. Dhar S, McConnell MP, Gharibjanian NA, Young CM, Rogers JM, Nguyen TD, Evans GR. Tissue Eng. 2007; 13:2357. [PubMed: 17624931]
28. Gilad AA, McMahon MT, Walczak P, Winnard PT Jr, Raman V, van Laarhoven HW, Skoglund CM, Bulte JW, van Zijl PC. Nat Biotechnol. 2007; 25:217. [PubMed: 17259977]
29. Liu G, Liang Y, Bar-Shir A, Chan KW, Galpoththawela CS, Bernard SM, Tse T, Yadav NN, Walczak P, McMahon MT, Bulte JW, van Zijl PC, Gilad AA. J Am Chem Soc. 2011; 133:16326. [PubMed: 21919523]
30. McMahon MT, Gilad AA, DeLiso MA, Berman SM, Bulte JW, van Zijl PC. Magn Reson Med. 2008; 60:803. [PubMed: 18816830]
31. Jones CK, Polders D, Hua J, Zhu H, Hoogduin HJ, Zhou J, Luijten P, van Zijl PC. Magn Reson Med. 2012; 67:1579. [PubMed: 22083645]
32. Rabenstein DL, Isab AA. Journal of Magnetic Resonance. 1979; 36:281.
33. Zhong JH, Gore JC, Armitage IM. Magnetic Resonance in Medicine. 1989; 11:295. [PubMed: 2550719]
34. Poptani H, Puumalainen AM, Grohn OH, Loimas S, Kainulainen R, Yla-Herttuala S, Kauppinen RA. Cancer Gene Ther. 1998; 5:101. [PubMed: 9570301]
35. Grohn OH, Valonen PK, Lehtimaki KK, Vaisanen TH, Kettunen MI, Yla-Herttuala S, Kauppinen RA, Garwood M. Cancer Res. 2003; 63:7571. [PubMed: 14633668]
36. Gambhir SS, Bauer E, Black ME, Liang Q, Kokoris MS, Barrio JR, Iyer M, Namavari M, Phelps ME, Herschman HR. Proc Natl Acad Sci U S A. 2000; 97:2785. [PubMed: 10716999]
37. Cohen B, Ziv K, Plaks V, Israely T, Kalchenko V, Harmelin A, Benjamin LE, Neeman M. Nat Med. 2007; 13:498. [PubMed: 17351627]
38. Genove G, Demarco U, Xu H, Goins WF, Ahrens ET. Nat Med. 2005; 11:450. [PubMed: 15778721]
39. Koretsky AP, Brosnan MJ, Chen LH, Chen JD, Van Dyke T. Proc Natl Acad Sci U S A. 1990; 87:3112. [PubMed: 2326269]
40. Walter G, Barton ER, Sweeney HL. Proc Natl Acad Sci U S A. 2000; 97:5151. [PubMed: 10805778]
41. Kodibagkar VD, Yu J, Liu L, Hetherington HP, Mason RP. Magn Reson Imaging. 2006; 24:959. [PubMed: 16916713]
42. Judenhofer MS, Wehrl HF, Newport DF, Catana C, Siegel SB, Becker M, Thielscher A, Kneilling M, Lichy MP, Eichner M, Klingel K, Reischl G, Widmaier S, Rocken M, Nutt RE, Machulla HJ, Uludag K, Cherry SR, Claussen CD, Pichler BJ. Nat Med. 2008; 14:459. [PubMed: 18376410]

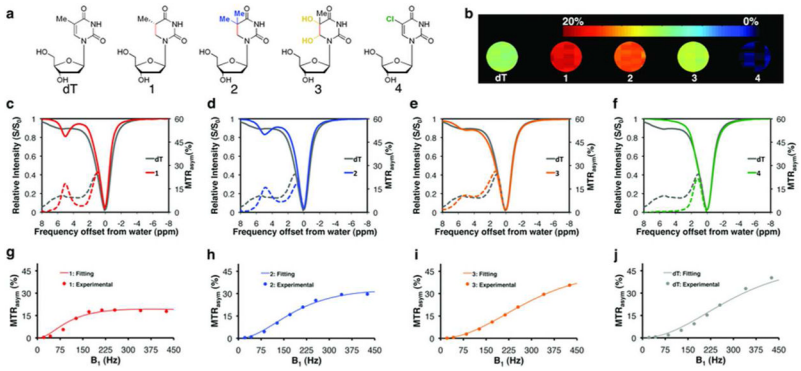

Figure 1. Evaluation of thymidine analogs as potential CEST agents

a) Chemical structure of dT and compounds **1–4**. b) MTR_{asym} maps of dT and **1–4** obtained at a 5ppm frequency offset from the water resonance. c–f) CEST-spectra (solid lines) and MTR_{asym} plots (dashed lines). A B_1=170 Hz was used for b–f. g–j) MTR_{asym} plotted as function of saturation power (B_1, Hz), experimental (dots), and QUESP-fitting (lines). In c–j, dT is plotted in gray, **1** in red, **2** in blue, **3** in orange, and **4** in green. Data were acquired at 11.7 Tesla, pH=7.4, and 37°C for 20 mM CEST-agent solutions. For **1–3,** MTR_{asym} values were calculated at 5 ppm (g–i), and for dT at 6 ppm (j).

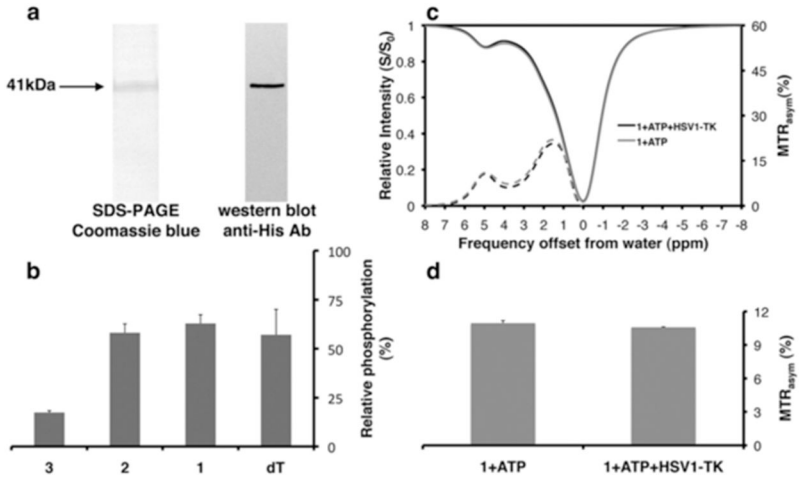

Figure 2. Expression, purification and activity of HSV1-TK

a) Coomassie Blue staining of SDS-PAGE and western blot analysis (anti-His antibody) of purified recombinant HSV1-TK. b) Relative phosphorylation of 5 μM of the indicated agent (dT, **1–3**) in the presence of pure recombinant HSV1-TK (a), as measured with the Kinase-Glo® assay. c) CEST-spectra (solid lines) and MTR_{asym} plots (dashed lines) obtained for the kinase reactions with (black lines) and without (gray lines) purified HSV1-TK enzyme for **1**. (d) MTR_{asym} (5ppm) values of **1** before (**1**+ATP) and after (**1**+ATP+HSV1-TK) phosphorylation (n=3). Relative phosphorylation is defined in the *Experimental section*.

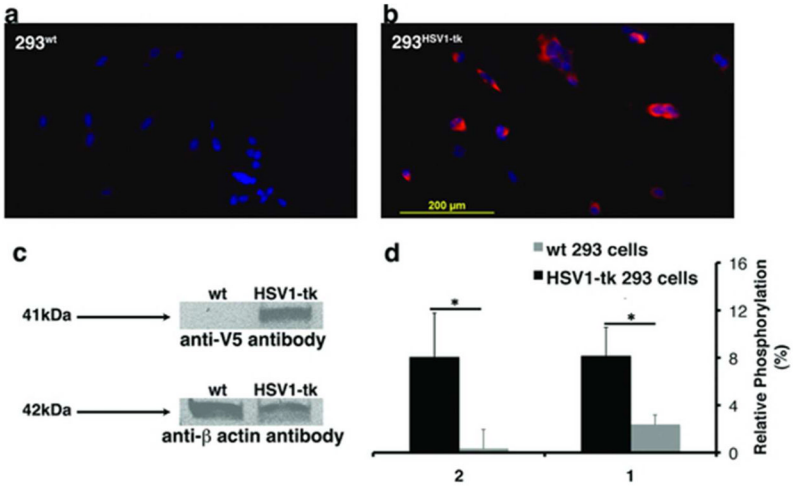

Figure 3. HSV1-TK specificity

Immunofluorescence of a) 293^{wt} and b) $293^{HSV1\text{-}tk}$ cells using anti-V5 antibody (red) for HSV1-TK staining overlaid on a DAPI staining (blue). c) Western blot of HEK293FT cell extracts using anti-V5 antibody, with staining for HSV1-TK-expressing (HSV1-tk) and wild-type (wt) cells. d) Relative phosphorylation of 5 μM of compounds **1** and **2** in the presence of 2μl cell extracts. Relative phosphorylation is defined in the *Experimental section*. * $p < 0.05$ (student's t-test, unpaired, two-tailed).

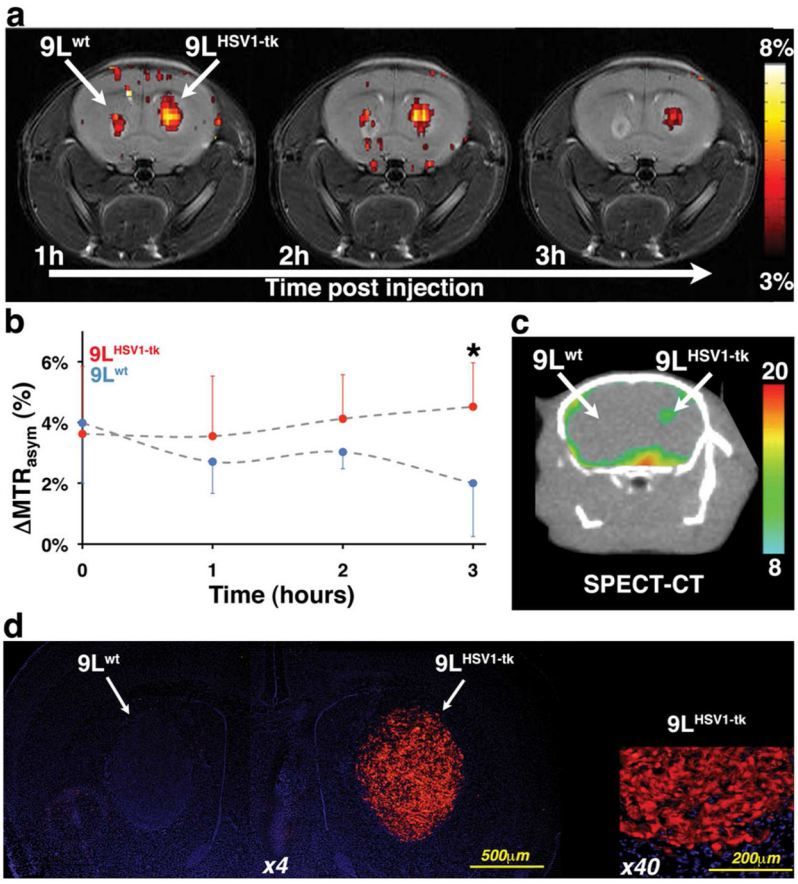

Figure 4. Imaging HSV1-TK expression

Left hemisphere: wild type 9L tumor ($9L^{wt}$); right hemisphere: 9L tumor expressing HSV1-TK ($9L^{HSV1\text{-}tk}$). a) Representative longitudinal *in vivo* MTR_{asym} (5 ppm) maps of the mouse brain overlaid on T_2-weighted images, showing the distribution of **2** obtained one hour, two hours, and three hours after i.v. injection. b) Temporal changes in the ΔMTR_{asym} values (mean ± s.d.) of each tumor type before (n=3) and after (n=8) i.v. administration of **2**. (* *p*-Value<0.01). c) Transverse views of co-registered SPECT-CT images of HSV1-TK expression, obtained three hours after i.v. injection of [^{125}I]FIAU. d) Immunostaining of perfused mouse brain section. Staining for HSV1-TK (anti-V5 antibody in red) overlaid on a DAPI staining (blue) at low (×4) and high (×40) magnifications.